N90-26222

TDA Progress Report 42-101 May 15, 1990

Inhomogeneous Electric Field Effects in a Linear RF Quadrupole Trap

R.K. Melbourne, J.D. Prestage, and L. Maleki
Communications Systems Research Section

This article presents the exact potential corresponding to confining fields inside a linear rf quadrupole particle trap of finite length. The analytic expression for the trapping potential is derived by introducing a linear trap employing a relatively simple cylindrical geometry and solving Laplace's equation for the trap electrodes. The finite length of linear traps results in field distortion near the trap ends. An exact analytic determination of the fields is useful because the profile of the trapped ion cloud is highly dependent on the fields confining it. It is shown that near the ends of the trap, the effective potential arising from the rf fields acts to propel particles out of the trap, and further, that the addition of a dc bias generates an inhomogeneous field in the trap that influences the particles both perpendicularly to and along the trap's long axis.

I. Introduction

Trapped $^{199}IIg^{+}$ ion standards are presently the most stable frequency standard developed for averaging times $\geq 10^4$ seconds. Trapped ions can be stored for long periods, essentially isolated from the outside environment. This arrangement serves to reduce the perturbation to the ions' atomic-energy levels and hence minimize frequency fluctuation.

Currently, the Time and Frequency Systems Research Group is developing a prototype linear ion trap consisting of four parallel cylindrical rod electrodes enclosed between two end electrodes (Fig. 1). This trap is preferable over the conventional spherical trap in frequency-standard applications because of its 20-times-larger ion storage capacity. The number of ions determines an important trade-off parameter between the signal-to-noise ratio and the second-order Doppler shift arising from the motion of the ions caused by the trapping field. The geometry of the linear trap improves clock peformance by allowing an increase of the number of trapped ions without degradation of the frequency stability [1].

Particle motion is directly affected by the electric fields generated within the trap. A time-varying quadrupole electric field is produced in the linear rf trap by an ac voltage applied to the four rods such that any rod's nearest neighbor has the opposite polarity. The rf field provides the trapping force necessary to confine particles in the radial direction (see Fig. 1). In order to prevent trapped particles from escaping out the ends of the trap, a dc voltage is applied to the two "endcaps," producing an exponentially

decaying field directed inward along the the axis of cylindrical symmetry of the trap (i.e, along the z axis). The linear trap is also capable of containing larger macroparticles (such as alumina or other substances) [2]. In this case, however, static electric fields must be incorporated in addition to the rf and endcap fields to offset gravitational forces on the macroparticles, which are comparable to the trapping forces. If the trap is oriented such that the trap axis is horizontal with the rods at the corners of a square when viewed down the trap axis, a dc voltage can be applied to the top two rods of the quadrupole to provide this offset.

RF fields in the radial direction of a linear trap have been analyzed extensively by assuming the trap to be infinitely long [3]. In actuality, however, the traps are of finite length, and thus both static and time-varying fields emanating from the rod electrodes will be directed longitudinally along the axis of the trap, as well as radially. Near the ends of the trap, field distortion occurs. In an ion trap, this can subsequently affect the shape of the trapped ion cloud and thus ion motion. To optimize clock performance, an exact determination of the fields generated within the trap, including the "end effects," is necessary. This then allows for the calculation of the surface shape of the ion plasma contained within the trap. In this article, an analytic model is developed for one implementation of a linear trap to determine static fields produced by the end electrodes and time-varying electric fields everywhere inside a finite-length linear trap with cylindrical geometry. The model consists of a hollow cylinder, partitioned lengthwise into four sections (analogous to the four rods) and two endcaps. The simple geometry of the cylinder allows the calculation of the fields within the cylinder accurately (Fig. 2).

Although consideration of a dc offset to counterbalance gravitational forces is unnecessary when modeling a linear trap designed for the storage of ions, it cannot be neglected when discussing a trap that contains macroparticles. The primary purpose of applying the dc offset is to counterbalance gravitational forces on macroparticles. However, if the bias is added to the rod electrodes, electric fields will be additionally generated along the axis of the trap in a manner that acts to longitudinally localize the particles in the trap center or to propel them out the ends of the trap, depending on the polarity of the dc offset. A second model is presented in this article to determine the effects of the fields generated by a dc voltage applied to two rods in the linear trap. Because the focus of this model is solely to demonstrate the effects of applying a dc offset to the trap, the contribution from the rf trapping fields and the fields generated by the end electrodes are neglected, although the complete determination of the potential inside a cylindrical macroparticle trap is possible by combining the potentials derived from the two models.

First presented is the conventional trapping theory for rf quadrupoles previously developed in the literature. Then, the potential everywhere inside a linear ion trap with cylindrical geometry is derived by modeling the trap after a four-sectioned hollow cylinder of finite length enclosed by two endcaps. In Section IV, the potential is determined inside a second model that consists of a hollow cylinder split along its length into two halves. The top half is at a voltage V_o and the bottom half and endcaps are grounded. This model accounts for the effect of a dc-offset potential applied to the rod electrodes in a linear macroparticle trap. The conclusion summarizes the results of the two models.

II. Trapping Theory

The linear trap typically employs two dc-biased "endcap" electrodes to confine the particles longitudinally, and four rods that produce a time-varying electric field to contain them in the transverse or radial direction. The voltage applied to the rods is such that at a given instant, any pair of adjacent rods always has opposite polarity (Fig. 3). The potential inside the trap near the central axis (i.e., $x, y \ll R$) is given by

$$V(x,y) = \frac{[V_o(x^2 - y^2)\cos(\Omega t)]}{2R^2} \tag{1}$$

where x and y denote the particle's position in the radial direction, R represents the distance between the central axis and the surface of the rods, and Ω is the driving frequency. The resultant time-varying electric fields produce a trapping force that increases linearly in the radial direction. A single charged particle within the trapping region will be subjected to a time-averaged force towards the central axis of the trap ($r = \sqrt{x^2 + y^2} = 0$) where the field intensity is a minimum. A nonzero time-averaged restoring force for a single particle is derivable from a pseudopotential, the effective potential existing in an inhomogeneous electric rf field [4]

$$\psi(x,y) = \frac{q[E_o(x,y)^2]}{4m\Omega^2} \tag{2}$$

In the case of an infinitely long linear trap, Eq. (2) modifies to

$$\psi(x,y) = \frac{qV_o^2}{4m\Omega^2 R^4}(x^2 + y^2) \tag{3}$$

where q is the charge on the particle and x and y are the particle's position in the radial direction averaged over one period $T = (2\pi/\Omega)$. The force generated from this pseudopotential produces particle dynamics that superimpose a slower oscillating motion characterized by frequency ω, upon a faster micromotion due to the driving frequency Ω. Stable confinement of the particles occurs when $\omega \ll \Omega$. The frequency ω for radial particle oscillation can be derived from Eq. (3) as

$$\omega^2 = \frac{q^2 {V_o}^2}{2m\Omega^2 R^4} \tag{4}$$

Although the particle is in dynamic equilibrium along the radial direction, it is still free to traverse the longitudinal (z) axis. If there is no constraining force along this axis and the trap contains more than one particle, the coulomb repulsion between the particles tends to propel them out the ends of the trap. To counterbalance these forces, dc-biased electrodes are incorporated at either end of the trap in both ion and macroparticle systems.

III. Analytical Model for the Potential Inside a Linear Trap

The complete electric field inside the linear ion trap consists of a static field arising from applied voltage on the endcaps and the time-varying fields resulting from a voltage arrangement on the trap rods. Unfortunately, the analytic determination of the net electric field for a finite-length four-rod linear trap is formidable and, as yet, only an approximation of the field exists by considering the trap to be infinitely long. This approximation neglects the effect trap ends have on the generated rf fields that influence the dynamics of trapped ions. Rather than neglecting the end effects, in the model described here the fields generated by the four-rod geometry are approximated by employing a hollow cylinder partitioned into four sections with endcaps at either end (Fig. 2). While providing a rough approximation to the four-rod trap, the model primarily represents a new linear-trap geometry that can be accurately modeled to determine the exact confining field, including any significant end effects. An exact analytic determination of the fields is highly useful since the shape of the trapped ion cloud depends strongly on the fields surrounding it. Because the ions contribute significantly to the electric field within the trap, only certain density profiles are acceptable. With a complete picture of the fields generated by the cylindrical shell and endcaps, Poisson's equation can be solved numerically to investigate the shape of the ion plasma. By virtue of its design, the cylindrical geometry also conveniently provides shielding against charge buildup that might occur in regions external to the trap such as lenses or mirrors. The pseudopotential arising from the rf fields and the potential generated from the endcaps are solved separately. Superimposing these two solutions produces the net potential everywhere inside the cylindrical trap.

The pseudopotential is determined by employing the four-sectored cylindrical model in Fig. 2 with grounded endcaps and a surface voltage V_o applied such that $V_o(\theta) = -V_o(\theta + \pi/2)$. This voltage arrangement represents the applied voltage on the four-rod quadrupole at a given instant. Starting with Laplace's equation in cylindrical coordinates, a general solution of the product form is assumed:

$$\Phi(r, \theta, z) = R(r)Q(\theta)Z(z) \tag{5}$$

It can be shown that for this type of geometry [5]

$$\Phi(r, \theta, z) = [A\cos(m\theta) + B\sin(m\theta)][CI_m(kr) + DK_m(kr)][E\sin(kz) + F\cos(kz)] \tag{6}$$

where I_m and K_m are the modified Bessel functions. The remaining coefficients are constants to be determined. With the requirements that $F, D = 0$ and

$$k_n = \frac{n\pi}{L} \tag{7}$$

the equation for Φ takes on the modified general form

$$\Phi(r, \theta, z) = \sum_{m=0}^{\infty}\sum_{n=0}^{\infty}\left[(A_{mn}\cos(m\theta) + B_{mn}\sin(m\theta))\left(I_m\left(\frac{n\pi r}{L}\right)\right)\left(\sin\left(\frac{n\pi z}{L}\right)\right)\right] \tag{8}$$

The asymmetric voltage is applied to the four cylinder sections on the cylindrical surface ($r = R$) such that:

$$V(\theta, z) = \left\{\begin{array}{ll} V_o, & -\pi < \theta < \frac{-\pi}{2} \\ -V_o, & \frac{-\pi}{2} < \theta < 0 \\ V_o, & 0 < \theta < \frac{\pi}{2} \\ -V_o, & \frac{\pi}{2} < \theta < \pi \end{array}\right\} \tag{9}$$

The potential on the surface is thus given as

$$V(\theta,z)=\sum_{m=0}^{\infty}\sum_{n=0}^{\infty}\Bigg[(A_{mn}\cos(m\theta)+B_{mn}\sin(m\theta))\left(I_m\left(\frac{n\pi R}{L}\right)\right)\times\left(\sin\left(\frac{n\pi z}{L}\right)\right)\Bigg] \quad (10)$$

with the coefficients

$$A_{mn}=0$$

$$B_{mn}=\frac{32V_o}{mn\pi^2}\left(I_m\left(\frac{n\pi R}{L}\right)\right)^{-1} \quad (11)$$

Substituting these constants back into Eq. (8), and multiplying Φ by $\cos(\Omega t)$ to take into account that it varies with a frequency Ω, the time-varying potential due to the surface voltage is determined:

$$\Phi=\frac{32V_o}{\pi^2}\sum_{m}^{\infty}\sum_{n}^{\infty}\left[\left(\frac{1}{mn}\frac{I_m\left(\frac{n\pi r}{L}\right)}{I_m\left(\frac{n\pi r}{L}\right)}\right)\times\sin(m\theta)\sin\left(\frac{n\pi z}{L}\right)\right]\cos(\Omega t) \quad (12)$$

where $m=2,6,10,\ldots$ and $n=1,3,5,\ldots$. Providing the secular frequency is much less than the frequency of micromotion ($\omega \ll \Omega$), the macromotion of the particle can be described by the time-independent pseudopotential discussed in Section II

$$\psi=\frac{q}{4m\Omega^2}(\nabla\Phi)^2 \quad (13)$$

and incorporating Eq. (12),

$$\psi=\frac{q}{4m\Omega^2}\left(A^2(r,\theta,z)+B^2(r,\theta,z)+C^2(r,\theta,z)\right) \quad (14)$$

where

$$A(r,\theta,z)=\frac{32V_o}{\pi L}\sum_{m}^{\infty}\sum_{n}^{\infty}\left[\frac{1}{m}\frac{I_m\left(\frac{n\pi r}{L}\right)}{I_m\left(\frac{n\pi R}{L}\right)}\times\sin(m\theta)\cos\left(\frac{n\pi z}{L}\right)\right]$$

$$B(r,\theta,z)=\frac{32V_o}{r\pi^2}\sum_{m}^{\infty}\sum_{n}^{\infty}\left[\frac{1}{n}\frac{I_m\left(\frac{n\pi r}{L}\right)}{I_m\left(\frac{n\pi R}{L}\right)}\times\cos(m\theta)\sin\left(\frac{n\pi z}{L}\right)\right]$$

$$C(r,\theta,z)=\frac{32V_o}{2L\pi}\sum_{m}^{\infty}\sum_{n}^{\infty}\left[\frac{1}{m}\times\frac{I_{m-1}\left(\frac{n\pi r}{L}\right)+I_{m+1}\left(\frac{n\pi r}{L}\right)}{I_m\left(\frac{n\pi R}{L}\right)}\times\sin(m\theta)\sin\left(\frac{n\pi z}{L}\right)\right] \quad (15)$$

The inhomogeneous electric field arising from this effective potential produces a net force on a single particle that, averaged over one period of the micromotion ($T=\Omega/2\pi$), is directed towards $r=0$ in the radial direction and out the ends of the trap in the z direction. The z dependence of the pseudopotential is demonstrated by Figs. 4(a) and 4(b), which represent examples of $\psi(z)$ at two different positions of θ. In both of the examples, $r=R/8$ with $V_{ac}=200$ V, $\Omega/2\pi=60$ Hz, $R=0.008$ m, and $L=0.06$ m. A 5 μm-diameter alumina particle with an approximate positive charge-to-mass ratio of 0.0053 C/kg is used to evaluate Eq. (14).

The magnitude of $\psi(\theta)$ for fixed values of r and z is sinusoidal and oscillates from a maximum in regions near the boundaries of each of the four sections of the cylinder ($\theta=0,\pi/2,\pi,2\pi$) to a minimum along the centers of the cylinder sections ($\theta=\pi/4,3\pi/4,5\pi/4,7\pi/4$) (Fig. 5). It is interesting to note that the pseudopotential in the cylindrical model indicates an electric field in θ that is actually 45 deg out of phase with the electric field generated in the linear four-rod trap. In the latter case, the pseudopotential is a maximum in the vicinity of the rods (located at $\theta=\pi/4,3\pi/4,5\pi/4,7\pi/4$) and a minimum between them. This discrepancy arises because the spatial separation of the rods results in weaker fields between any two rods in contrast to the fields between the cylinder sections whose boundaries meet and give rise to large electric fields. The fact that the pseudopotential is a minimum at the section centers in the cylindrical linear trap suggests that small viewing holes may be added in this vicinity without significant disturbance of the fields within.

In order to obtain the total potential inside the cylinder, the potential arising from the endcaps must be determined and superimposed on the pseudopotential. This is accomplished by solving Laplace's equation for a cylinder

with a grounded surface and endcaps held at a constant voltage V_e. The resulting potential inside the cylinder for this configuration is

$$\Phi_e(r,z) = 2V_e \sum_{m=1}^{\infty} \left[\frac{J_0\left(\frac{P_m r}{R}\right)}{P_m J_1(P_m)} \left(\frac{\cosh\left(\frac{P_m(z-L/2)}{R}\right)}{\cosh\left(\frac{P_m L}{2R}\right)} \right) \right] \tag{16}$$

where J_0 and J_1 are the *zero*th and first Bessel functions, respectively, and P_m is the mth root of J_0. Adding Eqs. (14) and (16) determines the net potential inside a finite cylinder of length L and radius R

$$\Psi_{net}(r,\theta,z) = \psi + \Phi_e \tag{17}$$

The net potential can be interpreted geometrically by observing that it is composed of the pseudopotential whose curve, as demonstrated in Figs. 4(a) and 4(b), rises for fixed values of r and θ from a minimum at $z = 0$ and $z = L$ to a maximum in the center of the trap, and an "endcap" potential that varies from a constant V_1 on the ends to a minimum in the center of the trap (Fig. 6). By controlling the amount of voltage applied to the endcaps, Ψ_{net} can be adjusted. The model suggests that there is an optimum endcap voltage that maximizes the continuity of the net potential in the z direction. Figure 7 demonstrates the z dependence of Ψ_{net} when Φ is greater than ψ.

IV. Analytical Model for a DC Field Perpendicular to the Cylindrical Axis

In a horizontal configuration, the introduction of a dc voltage on the top two rods of the linear quadrupole trap generally serves to counter the forces of gravity on macroparticles. Because the rods are of finite length, however, the electric field is not directed exclusively in the radial direction as in the case of infinite rod length. Instead, a distortion of the field lines occurs at the ends of the rods, giving rise to a field component in the longitudinal direction. The effects on particle dynamics of an asymmetric dc bias may be understood by again considering the four-rod quadrupole to be a hollow cylindrical trap split into two sections; the z axis is coincident with the axis of the linear quadrupole trap. Figure 8 depicts the cylindrical model with radius R and length L. To model the effects of the offset in the trap, a dc voltage is applied on the top half of the cylinder and the bottom half and endcaps are grounded. This potential can be added to Ψ_{net} developed in the previous section to provide a full solution of the potential inside a linear trap when a dc bias is added. The potential due to the dc offset is solved in a similar manner as the problem in Section II, and the results are

$$\Phi(r,\theta,z) = \frac{2V_o}{\pi} \sum_{n\ odd}^{\infty} \left[\left(\frac{\sin\left(\frac{n\pi z}{L}\right)}{n} \right) \left(\frac{I_0\left(\frac{n\pi r}{L}\right)}{I_0\left(\frac{n\pi R}{L}\right)} + \sum_{m\ odd}^{\infty} \frac{4}{m\pi} \frac{I_m\left(\frac{n\pi r}{L}\right)}{I_m\left(\frac{n\pi R}{L}\right)} \sin(m\theta) \right) \right] \tag{18}$$

Figure 9 represents a computer evaluation for this function of the first 22 values of m and n, respectively. Near the central axis of the trap ($r = 0$), the function varies smoothly, falling off to zero at $z = 0$ and $z = L$. The resultant electric field at $r = 0$ is

$$-\frac{\partial\Phi(r,\theta,z)}{\partial z} = E_z = \frac{-2V_o}{L} \sum_{n\ odd}^{\infty} \cos\left(\frac{n\pi z}{L}\right) \left[I_o\left(\frac{n\pi R}{L}\right) \right]^{-1} \tag{19}$$

The surface voltage V_o is inherently positive in Eq. (19). By referring to Figs. 10(a) and (b), it is evident that if a single negatively charged particle is subjected to this field, the force on that particle will be directed inward towards the center of the trap ($z = L/2$), growing abruptly from zero to a maximum as it approaches either end. The potential inside the trap could have been determined similarly by solving Laplace's equation for a voltage V_o applied to the bottom half of the cylinder instead of the top. In this case, if the particle had been taken to be positive, the net effect would still support the particle against gravity, but would accelerate the particle out one of the ends of the cylinder.

The analogy to the linear cylindrical trap is apparent. In order to counterbalance the gravitational effects on the particle, the dc voltage applied to the top rods must be of the opposite sign to that of the particle. But as demonstrated above, this condition inherently gives rise to an inhomogeneous force on the particle that is directed longitudinally inward, towards the center of the trap. Likewise, a gravitational offset can also be accomplished by applying a voltage to the bottom two trap rods that is the same polarity as the particle. This, however, additionally produces an electric field that acts to force the particle out the ends of the trap.

Farther out along the radial direction, the potential increases in magnitude and the function assumes a more rectangular shape. In the limit at $r = R$, V_o spans the

rectangular shape. In the limit at $r = R$, V_o spans the length of the cylinder and the function discontinuously jumps to 0 at either end. The electric field evaluated on the surface is

$$-\frac{\partial\Phi(\theta,z)}{\partial z} = E_z = -\frac{2V_o}{L}\sum_{n\ odd}^{\infty}\left[\cos\left(\frac{n\pi z}{L}\right)\right.$$

$$\left.\times\left(1+\frac{4}{\pi}\sum_{m\ odd}^{\infty}\frac{1}{m}\sin\left(\frac{m\pi}{2}\right)\right)\right] \quad (20)$$

where θ is again taken to be a constant at $\pi/2$. The model indicates that the electric field in the z direction towards the center of the trap depends on the radial position of the particle. This dependence is demonstrated by comparing Figs. 10(a) and (b).

The cylindrical model approximates the field accurately and yields insight into the influences on the particle in the longitudinal direction from the gravitational offset. For the case of many trapped particles, the model suggests that in some instances a bias on the end electrodes is not really necessary to counterbalance coulomb repulsion between particles, if a dc offset on the top rods is added. In this case, the particles will distribute themselves in such a manner as to create an equilibrium situation, balancing the coulomb forces and the force arising from the applied voltage.

V. Conclusion

This article has presented a model for the rf fields in a linear trap by considering a four-sector cylindrical geometry. This geometry approximates a finite linear trap with rod electrodes. It also represents a new configuration for an ion trap that is amenable to analytic determination of the confining fields. Using the model for the finite-length linear cylindrical trap, it was shown that confining fields have a longitudinal component as well as a radial component. The z component of the rf electric field produces an extra term in the pseudopotential not present in the ideal, infinitely long trap. The details of the end effects are important in ion confinement. The analytic model indicates that the pseudopotential arising from the rf fields gives rise to a time-averaged force towards the center of the trap in the radial direction and away from the center in the z direction. This latter effect, combined with the ions' own coulomb interaction, will accelerate the particles out of the trap if biased endcaps are not present. The density of the ion cloud can be determined numerically by solving Poisson's equation for the fields generated by the trap electrodes encompassing the ion plasma. Future research is planned for the evaluation of the plasma shape in a linear cylindrical trap.

When a dc bias potential is applied to the trap electrodes (for example, in the case of a macroparticle trap where the gravitational force is counterbalanced with a dc offset), an electric field is generated in both the radial and longitudinal directions. An analytic model has been developed that utilizes a cylindrical geometry to determine these fields. According to the model, a particle of the opposite sign to an applied dc voltage on the upper electrodes will feel an inwardly directed force along the z axis in addition to the transverse force. On the other hand, a particle with the same polarity as an applied dc voltage on the lower electrodes will be forced upwards in the transverse direction and towards the trap ends in the longitudinal direction.

Acknowledgment

The authors wish to acknowledge the use of the JPL Cray supercomputer to perform these simulations.

References

[1] J. D. Prestage, G. J. Dick, and L. Maleki, "New Ion Trap for Frequency Standard Applications," *J. Appl. Phys.*, vol. 66, no. 3, pp. 1013–1017, 1989.

[2] R. F. Wuerker, H. Shelton, and R. V. Langmuir, "Electrodynamic Containment of Charged Particles," *J. Appl. Phys.*, vol. 30, no. 3, pp. 342–349, 1959.

[3] G. R. Janik, J. D. Prestage, and L. Maleki, "Simple Analytic Potentials for Linear Ion Traps," *TDA Progress Report 42-99*, vol. July–September 1989, Jet Propulsion Laboratory, Pasadena, California, pp. 12–19, November 15, 1989.

[4] H. G. Dehmelt, "Radiofrequency Spectroscopy of Stored Ions, I: Storage," *Adv. At. Mol. Phys.*, vol. 3, pp. 53–154, 1967.

[5] J. D. Jackson, *Classical Electrodynamics*, 2nd edition, New York: John Wiley and Sons, Inc., 1975.

Fig. 1. Linear four-rod quadrupole trap.

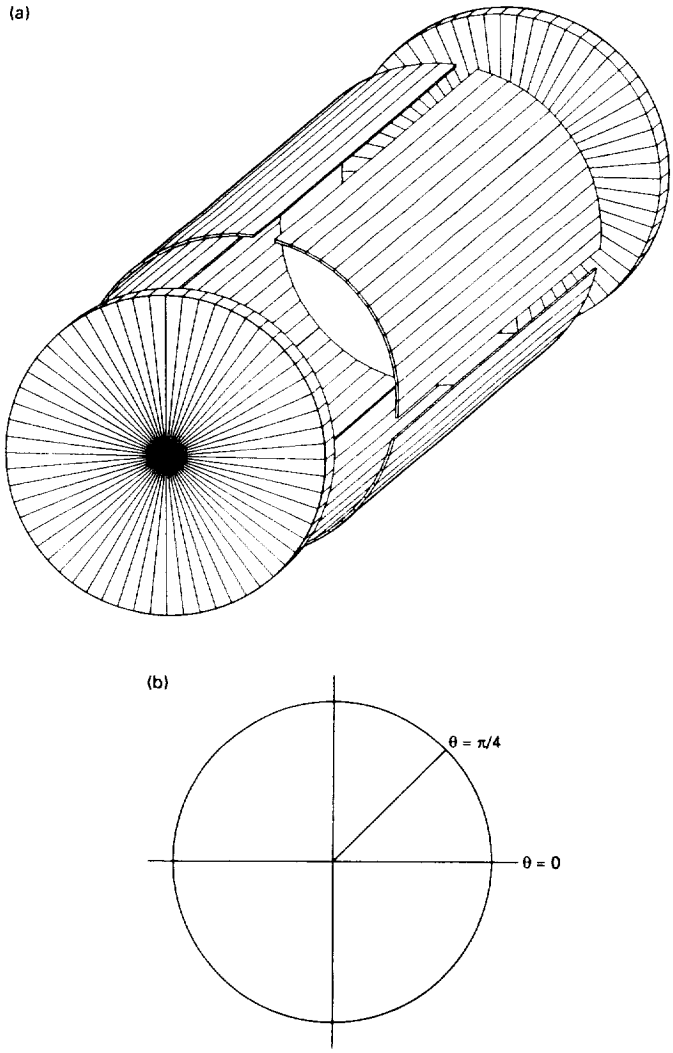

Fig. 2. Linear four-sectored quadrupole trap: (a) three-dimensional view of the trap with endcaps; and (b) orientation of the cylinder sections as viewed down the z axis. Section boundaries meet at $\theta = 0$, $\pi/2$, π, and $3\pi/2$.

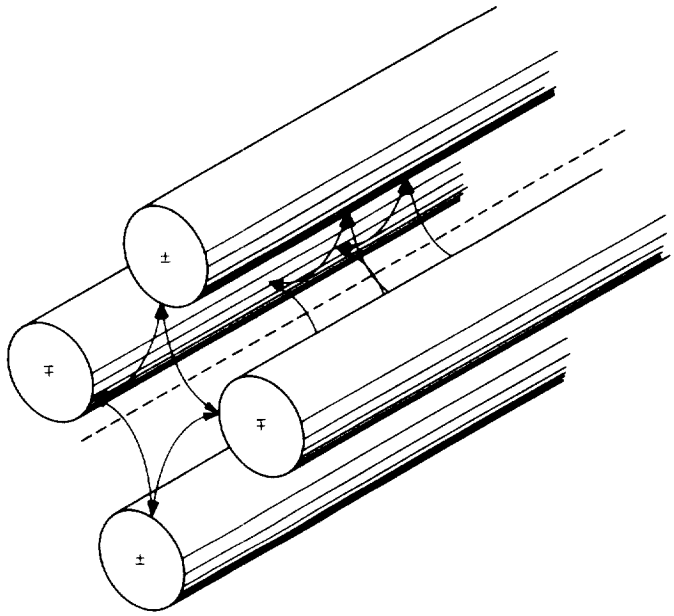

Fig. 3. Four-rod quadrupole. The voltage on each rod's nearest neighbor has opposite polarity.

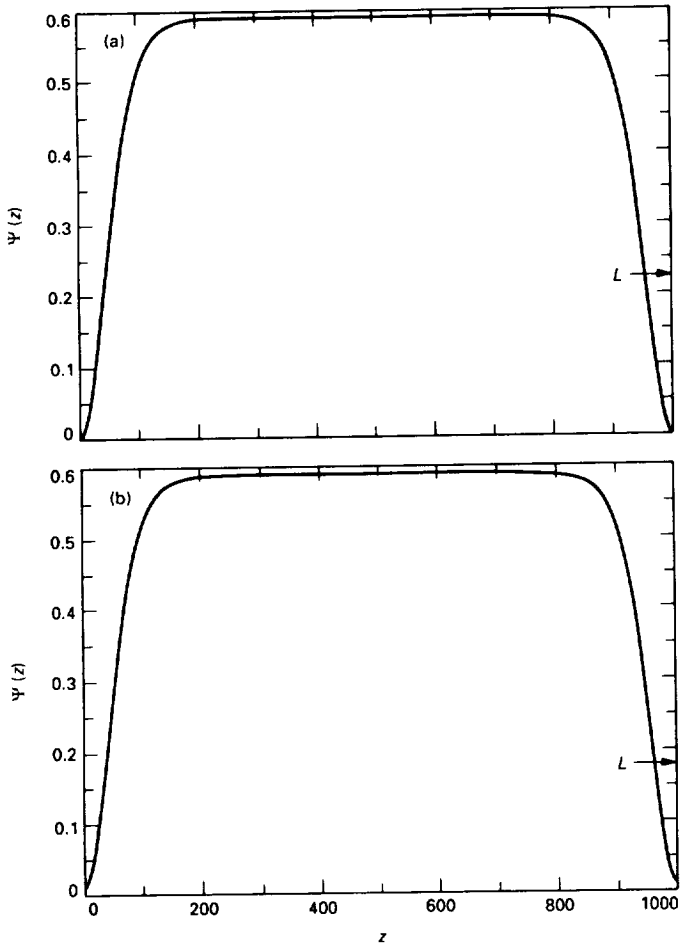

Fig. 4. The pseudopotential $\psi(z)$ at two positions of θ: (a) z dependence of $\psi(r,\theta,z)$ evaluated at $r = R/8$ and $\theta = 0$ for a single alumina particle with $e/m = 0.0053$ C/kg and trapping parameters $V_{ac} = 200$ V and $\Omega/2\pi = 60$ Hz; and (b) $\psi(r,\theta,z)$ evaluated at $r = R/8$ and $\theta = \pi/4$.

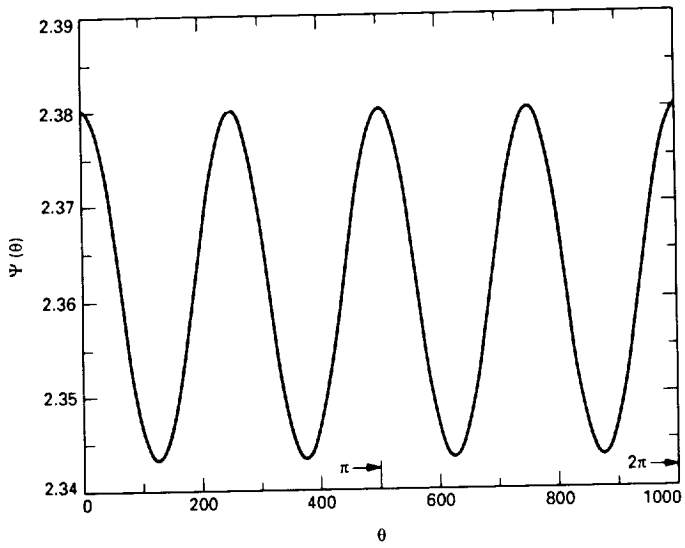

Fig. 5. Angular dependence of $\psi(r,\theta,z)$ evaluated at $r = R/4$ and $z = L/2$ for a single alumina particle with $e/m = 0.0053$ C/kg and trapping parameters $V_{ac} = 200$ V and $\Omega/2\pi = 60$ Hz.

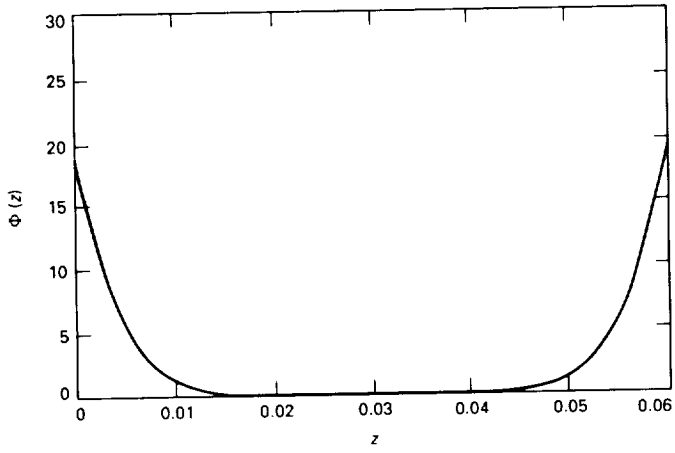

Fig. 6. The longitudinal (z) dependence of $\Phi_e(r,z)$ evaluated at $r = 0$ with end electrode voltage $V_1 = 20$ V.

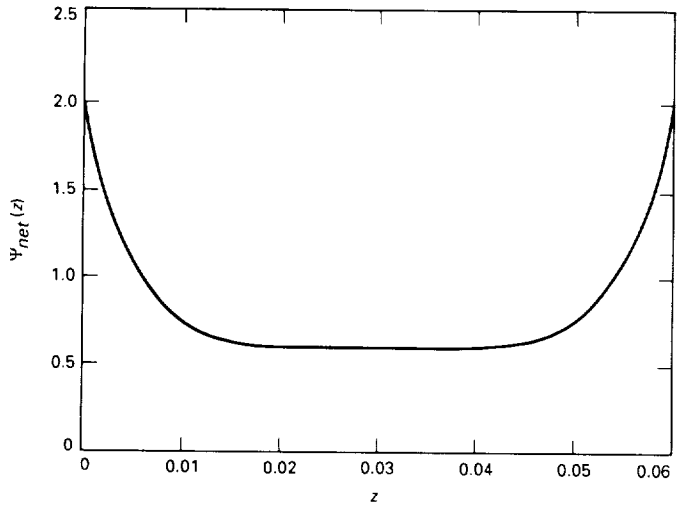

Fig. 7. The longitudinal *(z)* dependence of $\Psi_{net}(r,\theta,z)$ evaluated at $r = R/8$ and $\theta = \pi/4$ for a single alumina particle with $e/m =$ 0.0053 C/kg and trapping parameters $V_{ac} = 200$ V, $V_1 = 2$ V, and $\Omega/2\pi = 60$ Hz.

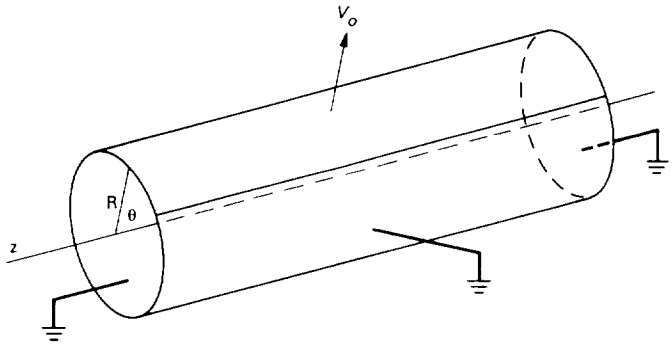

Fig. 8. Cylindrical model for a linear particle trap with a dc bias added to the top two rods of the trap.

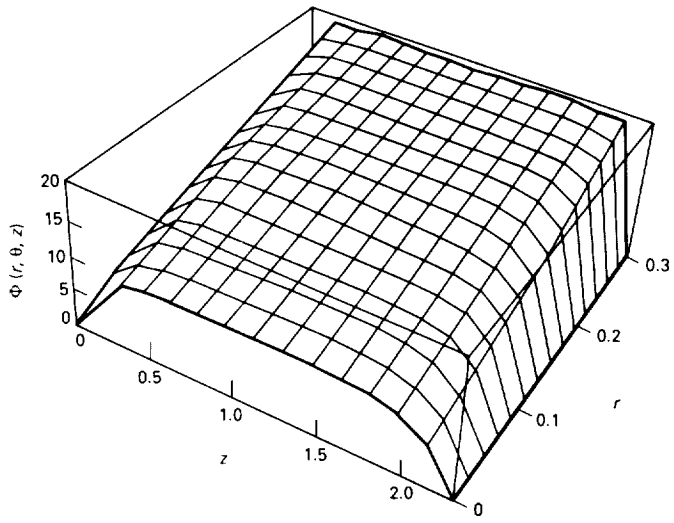

Fig. 9. The potential $\Phi(r,\theta,z)$ due to a dc offset inside the cylindrical model evaluated at $\theta = \pi/2$ with an applied voltage $V_o =$ 20 V.

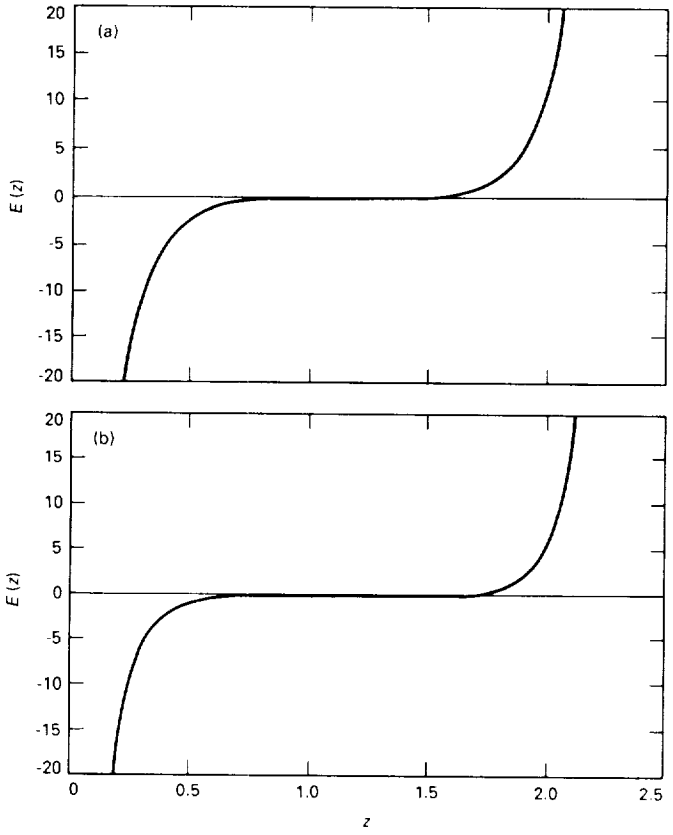

Fig. 10. The electric field $E(z)$ within the cylindrical model: (a) at a fixed $r = 0$, $\theta = \pi/2$, and $V_o = 20$ V; and (b) at a fixed $r = 3R/4$, $\theta = \pi/2$, and $V_o = 20$ V.